



Advanced Cu-Sn foam for selectively converting CO₂ to CO in aqueous solution



Jujin Zeng^{a,*}, Katarzyna Bejtka^a, Wenbo Ju^{b,*}, Micaela Castellino^a, Angelica Chiodoni^a, Adriano Sacco^a, M. Amin Farkhondehhal^c, Simelys Hernández^{a,c}, Daniel Rentsch^b, Corsin Battaglia^b, Candido F. Pirri^{a,c}

^a Center for Sustainable Future Technologies @POLITO, Istituto Italiano di Tecnologia, Via Livorno 60, 10144 Turin, Italy

^b Laboratory Materials for Energy Conversion, Swiss Federal Laboratories for Materials Science and Technology (Empa), Überlandstrasse 129, 8600 Dübendorf, Switzerland

^c Department of Applied Science and Technology, Politecnico di Torino, C.so Duca degli Abruzzi 24, 10129 Turin, Italy

ARTICLE INFO

Keywords:

Carbon dioxide
Electrochemical reduction
Catalyst
Copper-tin foam
Dendrite structure

ABSTRACT

A tin-modified copper foam for the efficient and selective reduction of CO₂ to CO is reported. We employ a cost-efficient electrodeposition route to form a three-dimensional porous dendrite architecture, in which each dendrite possesses a copper core and a copper oxide/tin oxide shell. The sparse tin species on the electrode surface play a key role to achieve excellent faradaic efficiencies for CO formation with a maximum value of 94%. We demonstrate high CO partial current densities of 4.7 mA cm⁻² and 7.9 mA cm⁻² at applied potentials of -0.8 V and -1.1 V vs. the reversible hydrogen electrode, respectively. The high activity for electrochemical CO₂ reduction is attributed to the unique hierarchical porous structure, which offers abundant electrochemically active sites and facilitates mass transport.

1. Introduction

With the aim to close the carbon cycle and compensate anthropogenic carbon dioxide (CO₂) emissions, many strategies have been proposed for CO₂ reduction, including thermochemical, photochemical, and electrochemical approaches [1–4]. Among these methods, electrochemical CO₂ conversion is of particular interest, since it can be carried out under ambient conditions with water (H₂O) as the only additional feedstock besides CO₂. The reaction rate and type of products are controlled by tuning the external bias and applied electrocatalysts [5]. In addition, electricity generated from renewable sources may be employed to achieve a fully sustainable route and provide a solution for seasonal energy storage [6].

The CO₂ reduction reaction (CO₂RR) involves several proton-assisted multiple-electron-transfer processes with similar equilibrium potentials, capable of generating carbon monoxide (CO, -0.11 V vs the reversible hydrogen electrode, RHE), formic acid (HCOOH, -0.22 V vs RHE), methane (CH₄, +0.17 V vs RHE), ethylene (C₂H₄, +0.08 V vs RHE), methanol (CH₃OH, +0.03 V vs RHE) and other products [7]. In addition, the hydrogen evolution reaction (HER, 0 V vs RHE) competes

with CO₂RR in aqueous solutions. While it is consequently challenging to control the selectivity of the CO₂ electroreduction from a thermodynamic point of view, it is even more challenging when considering kinetics [8]. Thus, effective catalyst design is essential to reduce the overpotentials and to drive efficiently the CO₂RR.

Carbon monoxide (CO) is one of the most desired products from the CO₂RR, since it can be further converted to oxygenates and hydrocarbons through the Fischer-Tropsch process [7,9,10]. Silver (Ag) and gold (Au) are intensively investigated electrocatalysts for selectively reducing CO₂ to CO [11,12]. Copper (Cu), as a member of coinage metals, shows unique features of electrochemically converting CO₂ to a range of chemicals including hydrocarbons [13,14], but its selectivity for CO is low. However, the selectivity of Cu can be tuned towards CO by introduction of a secondary metal, such as indium (In), tin (Sn), Ag, or aluminum (Al) [15–19]. Takanabe et al. [17] reported that a Cu-based electrocatalyst prepared by electrodeposition of Sn on thermally oxidized Cu foil shows outstanding selectivity towards CO (CO faradaic efficiency (FE_{CO}) > 90%) at low and moderate overpotentials. However, this Cu-Sn catalyst shows relatively low geometric current densities, which are about 1.0 mA·cm⁻² at -0.6 V vs. RHE, and

* Corresponding authors.

E-mail addresses: jujin.zeng@iit.it (J. Zeng), katarzyna.bejtka@iit.it (K. Bejtka), wenbo.ju@empa.ch (W. Ju), micaela.castellino@iit.it (M. Castellino), angelica.chiodoni@iit.it (A. Chiodoni), adriano.sacco@iit.it (A. Sacco), mohammadamin.farkhondehhal@polito.it (M.A. Farkhondehhal), simelys.hernandez@polito.it (S. Hernández), daniel.rentschi@empa.ch (D. Rentsch), corsin.battaglia@empa.ch (C. Battaglia), fabrizio.pirri@polito.it (C.F. Pirri).

$3.1 \text{ mA} \cdot \text{cm}^{-2}$ at -0.8 V vs. RHE. Wallace et al. [20] reported Sn-nano-particle-decorated Cu oxide nanowires featuring high FE_{CO} up to 82% and a CO partial current density of $4.5 \text{ mA} \cdot \text{cm}^{-2}$ at -0.8 V vs. RHE. Sun et al. [21] synthesized monodisperse Cu/SnO₂ nanoparticles via a seed-mediated method by the thermal decomposition of Sn(II) acetylacetone in the presence of Cu nanoparticles, and found that Cu/SnO₂ nanoparticles supported on carbon paper achieve an excellent FE_{CO} of 93% at -0.7 V vs. RHE with a current density of $4.6 \text{ mA} \cdot \text{cm}^{-2}$. However, such Cu-Sn materials usually require a complex multi-step synthesis procedure and their deposition on the carbon supports adds a further step to the fabrication process.

Here we present a low-cost scalable electrodeposition process for the fabrication of a Sn-modified porous Cu foam catalyst for the reduction of CO₂ to CO. We show that the hybrid foam consists of a three-dimensional porous dendrite architecture, in which each dendrite possesses core-shell structure. Electrochemical measurements demonstrate excellent CO selectivity and high activity and stability of this catalyst in aqueous electrolyte.

2. Experimental

2.1. Materials

Copper foil (Cu foil 99.99%, 0.25 mm thick) was purchased from Goodfellow. Tin foil (Sn foil 99.95%, 0.25 mm thick) was purchased from Advent Research Materials Ltd. Tin(II) chloride dihydrate ($\text{SnCl}_2 \cdot 2\text{H}_2\text{O}$, 99.9%), copper(II) sulfate pentahydrate ($\text{CuSO}_4 \cdot 5\text{H}_2\text{O}$, 99.0%), sulfuric acid (H_2SO_4 , 98%), potassium hydroxide (99.995% metal basis, Merck) and potassium bicarbonate (KHCO_3 , 99.7%) were purchased from Sigma-Aldrich. Unless otherwise specified, all the materials were used as received in this work.

2.2. Electrode preparation

2.2.1. Fabrication of Cu foams

Cu foils (dimension of $1 \times 1 \text{ cm}^2$) were sonicated in acetone, and then rinsed thoroughly with deionized water to remove impurities. Galvanostatic electrodeposition of Cu foams was carried out in an electrochemical cell with two-electrode configuration. A platinum (Pt) foil of 2 cm^2 was used as the counter electrode. A solution of 0.5 M H₂SO₄ and 0.05 M CuSO₄ was used as electrolyte. A constant geometric current density of $0.26 \text{ A} \cdot \text{cm}^{-2}$ was applied in various electrodeposition durations, namely 2.5, 5, 10, and 20 min. The obtained Cu foams were denoted according to the deposition duration as Cu2.5, Cu5, Cu10, and Cu20, respectively. The Cu10 sample was further modified with Sn, as described in the Section 2.2.2.

2.2.2. Fabrication of Sn-modified Cu electrode

Sn was electrodeposited onto the as-prepared Cu10 foam in a cell with a two-electrode configuration. A Sn foil of 2 cm^2 was used as the counter electrode. A solution of 0.05 M SnCl₂ and 2 M KOH was used as electrolyte. The electrodeposition was carried out at a constant potential of -0.5 V for 30 s. The obtained Sn-modified Cu10 electrode was rinsed with deionized water.

2.3. Physical and chemical characterization

Field emission scanning electron microscopy (FESEM, ZEISS Auriga) was used to analyze the electrode morphology. X-ray diffraction (XRD) was performed in Bragg-Brentano symmetric geometry by using a PANalytical X'Pert Pro instrument (Cu-K α radiation, 40 kV and 30 mA) equipped with an X'Celerator detector. Transmission electron microscopy (TEM) observations were performed with a FEI Tecnai F20ST microscope, equipped with a field emission gun operating at 200 kV. High-angle annular dark field (HAADF) and energy dispersive X-ray spectroscopy (EDX) detectors were used in Scanning TEM (STEM)

mode. X-ray photoelectron spectroscopy (XPS) was carried out by using a PHI 5000 VersaProbe (Physical Electronics) system. The X-ray source was a monochromatic Al K α radiation (1486.6 eV). Spectra were analyzed using Multipak 9.7 software. All core-level peak energies were referenced to C1s peak at 284.5 eV (C-C/C-H) and the background contribution in high resolution (HR) scans was subtracted by means of a Shirley function.

2.4. Electrochemical measurements

Before each electrochemical measurement, the electrode was in-situ reduced at -0.8 V vs. RHE for 20 min until a constant current was achieved. Unless otherwise specified, all the potentials were referred to RHE in this work.

Cyclic voltammetry (CV) and electrochemical impedance spectroscopy (EIS) were performed in a three-electrode cell at room temperature with a CHI760D electrochemical workstation. The working electrode was an as-prepared foam. A Pt wire was used as the counter electrode and a leakless miniaturized Ag/AgCl electrode (RE-1S, ALS) was used as the reference electrode. The electrolyte was a N₂- or CO₂-saturated 0.1 M KHCO₃ aqueous solution. EIS analysis was carried out at various applied constant potentials (from -0.2 to -1.0 V) with small signal amplitude of 10 mV and frequency range of $10^{-1} - 10^4 \text{ Hz}$. The CV was performed from -1.0 V to 0.4 V at a scan rate of 10 mV s^{-1} . To determine the double-layer capacitance of the electrode, CV was executed in a potential range of 0.02 V-0.22 V at scan rates of 5 mV s^{-1} , 10 mV s^{-1} , 25 mV s^{-1} and 50 mV s^{-1} in the N₂-saturated 0.1 M KHCO₃ aqueous solution.

The CO₂RR experiments were conducted in a custom-made two-compartment cell with a proton exchange membrane (Nafion™ Membrane N117, Sigma-Aldrich) as the separator. The volume of the electrolyte was approximately 8 ml in each of the two compartments, and the gas headspace was about 2 ml above the electrolyte on each side. The chronoamperometric measurements (CAs) were carried out by using a potentiostat (VersaSTAT 4, Ametek), with a leakless miniaturized Ag/AgCl electrode (ET072-1, eDAQ) as the reference and Pt gauze (2 cm^2 , 99.9%, MaTecK) as the counter electrode. 0.1 M KHCO₃ aqueous solution was used as electrolyte. Before each experiment, both the compartments were purged by CO₂ (99.998%, Messer) with a flow rate of 24 ml min^{-1} for 1 h to ensure a pure CO₂ atmosphere. The gas flow in the purging mode was regulated by a mass flow controller (Red-y MFC, Voegtlin). During the electrolysis experiments, CO₂ was introduced with a constant flow rate of 30 ml min^{-1} in order to ensure sufficient CO₂ transport to the electrode surface, while preventing interference from gas bubbles striking the surface. Each electrolysis experiment was performed at a fixed potential and the accurate potential was obtained by compensating the given potential with the ohmic potential drops in the system (IR-compensation). Gas chromatograph (μGC, INFICON) with a thermal conductivity detector (TCD) was used to determine the concentrations of gaseous products, and ¹H nuclear magnetic resonance (Avance III 400 NMR spectrometer, Bruker) spectra were used to quantify the liquid phase products.

3. Results and discussion

3.1. Fabrication and characterization of Cu and Cu-Sn foams

Cu foams are electrochemically deposited in an acidic solution at a current density of $0.26 \text{ A} \cdot \text{cm}^{-2}$. Because intense HER takes place at the applied potential, H₂ gas bubbles form on the electrode surface, and serve as a template for the Cu electrodeposition. Due to the random nucleation, growth and detachment of H₂ bubbles, the orientation of the growth of Cu deposits is continuously altered, resulting in porous foam structure. As shown in Figure S1 of supporting information (S.I.), the average pore size becomes larger with the increase of deposition time, caused by the coalescence of H₂ bubbles, which agrees with the

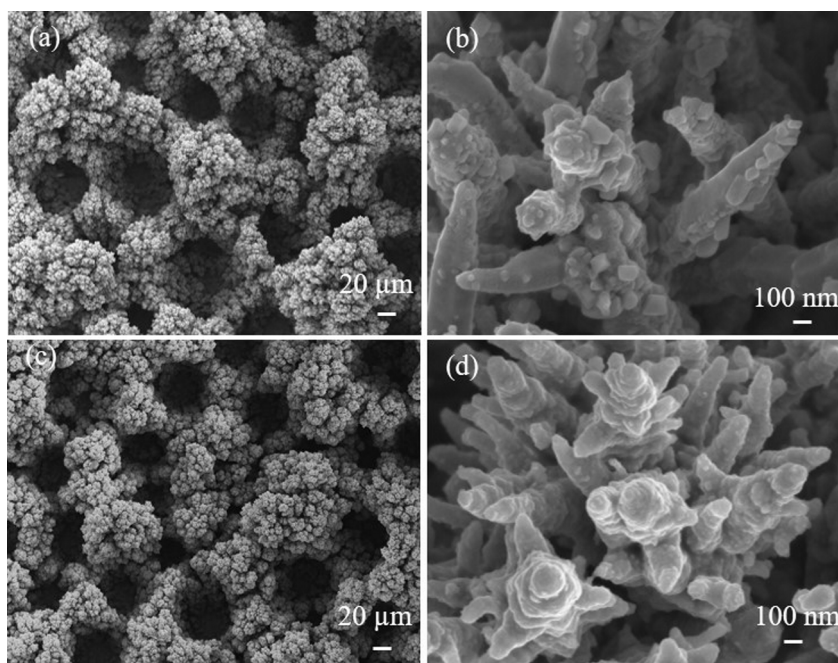


Fig. 1. FESEM images of (a, b) Cu foam and (c, d) Cu-Sn foam.

literatures [22,23]. The samples deposited for 2.5, 5, 10, and 20 min are named as Cu2.5, Cu5, Cu10, and Cu20, respectively.

The three-dimensional foam provides a large amount of electrochemical surface area (ESA), which can be evaluated by the measurement of the corresponding double-layer capacitance (C_{dl}) value [24,25]. As shown in Figure S2 of S.I., all Cu foams have enhanced C_{dl} values ($10.0\text{--}12.6\text{ m F cm}^{-2}$) as compared to the flat Cu foil ($28\text{ }\mu\text{F cm}^{-2}$). Cu10 foam shows a larger ESA (approximately 450 cm^2) than other foams (357 cm^2 and 375 cm^2 for Cu5 and Cu20, respectively). The ESA of Cu20 is smaller than that of Cu10, which can be attributed to the collapse and peel-off of the porous structure in a long-time deposition. In further study, Cu10 foams (hereafter Cu foam species Cu10 foam) are modified with Sn to get Cu-Sn foams.

As shown in Fig. 1a and c, the Cu-Sn foam ideally maintains the morphology of the Sn-free one. Both foams have three-dimensional open porous foam-like structure with an average pore size of approximately $80\text{ }\mu\text{m}$. The foam walls consist of numerous dendrites, which bear an apparent resemblance to a stag-horn coral-like structure (Fig. 1b and d). The size of the dendrites is hundreds of nanometers.

XRD patterns of Cu and Cu-Sn foams are shown in Fig. 2. The pattern of Cu foam displays the main peaks for both Cu (Copper, JCPDS 00-

004-0836) and Cu₂O (Cuprite, JCPDS 00-005-0667) crystalline phases. The peaks for Cu₂O are very low in intensity, giving evidence of a small quantity of Cu₂O in the Cu foam. A similar XRD pattern is observed on the Cu-Sn foam. No peak indicates the existence of crystalline Sn species, which can be attributed to their low quantity below the instrument detection limit, or to their non-crystalline phase.

Fig. 3a shows a typical HAADF-STEM image of the Cu-Sn dendrites. These dendrites have a hierarchical structure, and are terminated with smaller and thinner branches. A higher magnification image (in Fig. 3b) clearly shows the presence of nanoparticles on the surface of the branches, as partially visible by FESEM (in Fig. 1d). The bright-field TEM image gives further insight into the morphology of a single branch, which indicates a crystalline core covered by many nanoscale crystals (in Fig. 3c). Higher magnification of the border of the branch is shown in Fig. 3d, and the fast Fourier transform (FFT) image is also inset. According to the calculated interplanar distances, the ring patterns correspond to the randomly oriented Cu₂O nanocrystals. The existence of crystalline Cu₂O in the Cu-Sn foam is in agreement with the XRD analysis. To further shed light on the crystalline composition of this sample, selected area electron diffraction (SAED) of a small part of the single branch has been applied, and the image is inset in Fig. 3c. Two superimposed and well-defined diffraction patterns can be observed. The first is composed of rings, i.e. the diffraction pattern of polycrystalline Cu₂O, while the second is a diffraction pattern composed of bright spots, which is identified with Cu single crystal in [001] zone axis. Only Cu₂O can be observed on the surface of the branches, and the core is metallic Cu. The pattern of SAED of a large area (shown in Figure S3a of S.I.) reveals the existence of polycrystalline Cu and Cu₂O. However, Sn-related species are not observed, which agrees with the XRD analysis. Although crystalline Sn and SnO_x are not detected with XRD and SAED, the presence of Sn element is verified by EDX (in Figure S3b of S.I.). From the above-mentioned analyses, it is clear that the core of the dendrite is composed of metallic Cu solely and the outer layer of the dendrite is composed of Cu and Sn species.

XPS measurements are performed on the Cu-Sn foam to investigate the oxidation state of elements on the surface. From the survey spectrum (not reported), C, O, Cu, as well as a small amount of Sn (2.2 at. %) are detected. The atomic Cu/Sn ratio is 8.9. The Cu2p doublet region acquired in HR mode (see Fig. 4a) shows a typical structure which

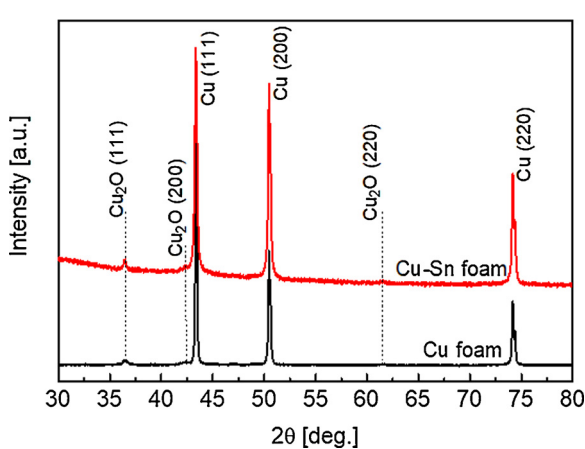


Fig. 2. XRD patterns of the Cu and Cu-Sn foams.

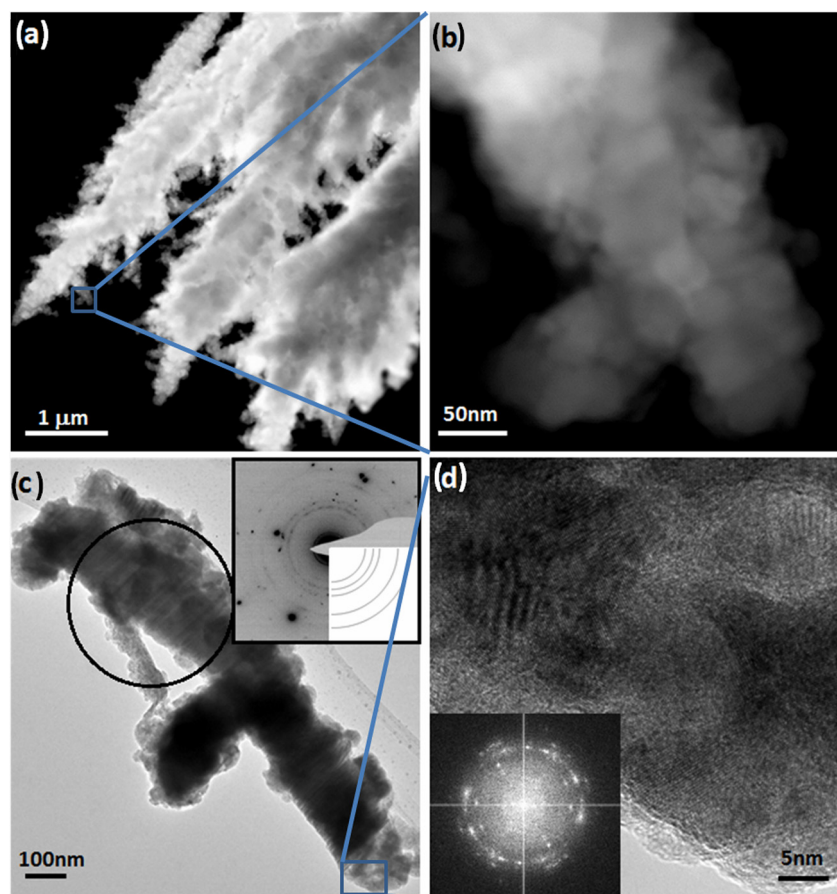


Fig. 3. TEM characterization of the Cu-Sn foam: (a, b) STEM images at lower and higher magnification; (c) BF-TEM image with corresponding SAED (inset); (d) HRTEM image of the border of the branch with corresponding FFT (inset).

could be related to the mixed oxidation states of Cu, including Cu(0), Cu(I) and Cu(II) [26]. Cu(0) and Cu(I) states are already observed with XRD and TEM analyses, while Cu(II) is absent in the diffraction analyses, probably due to its trace amount or its amorphous phase on the electrode surface. A thin CuO layer can spontaneously form when the sample is taken to ambient conditions even for a very short period of time [27]. Since the Cu2p peak is quite tricky to be deconvoluted, due to both the presence and overlapping of several satellites and shake-up peaks for each oxidation state, the Auger CuL₃M_{4,5}M_{4,5} region is also acquired (inset in Fig. 4a), in order to get more information. The position of the peak maximum (in the Kinetic Energy scale), equivalent to 916.9 eV, is typical of Cu(I) [28], which corresponds to the average oxidation state (AOS) in the Cu2p HR spectrum. The modified Auger parameter (1849.3 eV) is also in accordance with this observation. The Sn3d doublet (see Fig. 4b) shows the Sn3d_{5/2} maximum at 486.2 eV which is related to the presence of Sn(II) oxide, together with a small shoulder at 485.0 eV due to metallic Sn(0) [29]. Hence, both Cu and Sn elements on the surface of the hybrid foam show a metal-oxide coexistence, with a dominant concentration of the oxide phase.

According to the FESEM, XRD, TEM and XPS analyses, the Sn-modified Cu foam has open porous structure with an average pore size of approximately 80 μm. The foam walls consist of numerous dendrites, and each dendrite has a metallic Cu core and a CuO_x/SnO_x shell. The definition of a core-shell structure is consistent with the method of the preparation of the materials. During the first step of Cu electrodeposition, metallic Cu dendrites are formed in highly acidic environment. The CuO_x on the outer layers of Cu dendrites can be attributed to the exposure to air [23] or to the oxidation in aqueous solution at the terminal of Cu electrodeposition [22,24,27]. During the second step of Sn electrodeposition, a controlled small amount of SnO_x is added onto

the Cu dendrites. Since the chemical composition is distinct in the core and on the surface of the dendrites, it is appropriate to define that the dendrite has a core-shell structure, in which the core is metallic Cu and the shell is CuO_x/SnO_x.

3.2. Electrochemical properties of Cu and Cu-Sn foams

Fig. 5a and b show the CVs in both CO₂- and N₂-saturated electrolytes on the Cu and Cu-Sn foams, respectively. In the negative potential range, Cu foam in the CO₂-saturated electrolyte has a lower current density than that in the N₂-saturated one. Moreover, the onset potential for reduction reactions shifts negatively in the CO₂-saturated electrolyte. These observations are in agreement with the reported results on Cu materials for the CO₂RR [30,31]. The CVs of the Cu-Sn electrode are shown in Fig. 5b. The most obvious feature is a set of redox peaks attributed to the reduction (in the cathodic scan) and oxidation (in the anodic scan) of Sn species on the electrode surface [29]. In contrast with the Cu electrode, the Cu-Sn foam displays a higher current density in the CO₂-saturated electrolyte than in the N₂ one at the same potential. The opposite behavior of the two electrodes in the two atmospheres indicates the different catalytic selectivity of the two foams. In the N₂-saturated electrolyte where only HER occurs, Cu-Sn foam shows a more than three-fold decrease in the current density and a negative shift of 340 mV in the onset potential (where $i = 1.0 \text{ mA cm}^{-2}$) as compared to the Cu foam, which suggest lower intrinsic activity towards the HER on the former.

A detailed EIS analysis has been performed to understand the charge transfer behavior of both electrodes during the reduction reactions. Fig. 6a shows the Nyquist plots for a Cu-Sn foam measured at different potentials in the CO₂-saturated electrolyte. When the applied potential

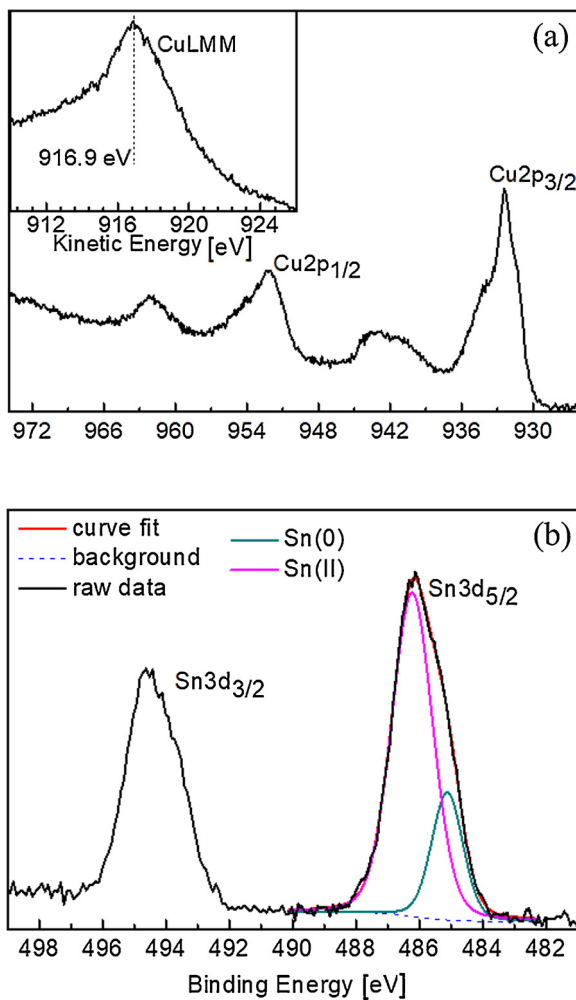


Fig. 4. XPS analysis on the surface of the Cu-Sn foam: (a) Cu2p doublet region acquired in HR mode and the Auger CuL₃M_{4,5}M_{4,5} region (inset); (b) High resolution Sn 3d XPS spectra.

becomes more negative, the impedance module value decreases, indicating higher faradaic reaction rates on the electrode surface. Spectra with similar features are obtained on the Cu-Sn foam in the N₂-saturated electrolyte as well as on the Cu foam in both N₂- and CO₂-saturated electrolyte (data not shown). Impedance data acquired for both samples in both atmospheres at -0.6 V are compared in Fig. 6b. The Cu foam exhibits lower impedances in both atmospheres than the Cu-Sn foam. Additionally, the Cu foam in the N₂ atmosphere has lower impedance than that in the CO₂ atmosphere. On the contrary, the Cu-Sn foam exhibits lower impedance in the CO₂ atmosphere than that in the N₂ one. EIS data are fitted through the equivalent circuit shown in the inset of Fig. 6b, composed of a series resistance R_s (associated to electrolyte resistance), a parallel between the resistance R₁ and the constant phase element Q₁ [32] (accounting for transport properties inside the catalyst), and another parallel R₂/Q₂ (related to the reduction reactions). The simulated spectra (solid lines) are superimposed on the experimental data shown in Fig. 6a and b. For what concerns series resistances and mass transport-related parameters, similar features are observed for both electrodes, namely R_s values in the range of 30–33 Ω, R₁ values of about 6–7 Ω, and Q₁ values in the range of 0.9–1.1 mF cm⁻² with negligible dependence on the potential and on the atmosphere. The double layer capacitance Q₂ is found to be about 11 mF cm⁻² for the Cu electrode, which is comparable to that obtained from the aforementioned CV evaluation (12.6 mF cm⁻²), and 5 mF cm⁻² for the Cu-Sn electrode. This result implies that the Sn deposition leads to

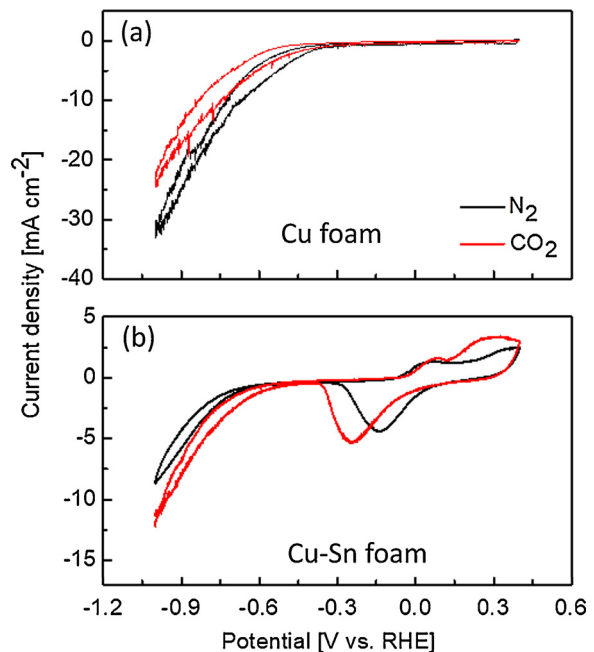


Fig. 5. CVs on the Cu and Cu-Sn electrodes in N₂- and CO₂-saturated 0.1 M KHCO₃ aqueous solution at a scan rate of 10 mV s⁻¹: (a) Cu foam; (b) Cu-Sn foam.

about one-fold decrease in the ESA. The charge transfer resistance R₂ is quite sensitive to applied potential and atmosphere, as shown in Fig. 6c. In the N₂-saturated electrolyte, Cu-Sn foam shows R₂ values 4–8 times as large as those for the Cu foam at potentials lower than -0.4 V, where the faradaic reaction is only HER. Hence, the specific charge transfer rate on the Cu foam is 2–4 times as high as those on the Cu-Sn one, considering that the ESA of the former is twice of the later. The low activity of the Cu-Sn foam for the HER obtained from the EIS analysis agrees very well with the CV measurements in the N₂-saturated electrolyte. Therefore, Sn modification has effectively suppressed the HER. In the CO₂-saturated electrolyte, both the HER and the CO₂RR occur competitively at potentials lower than -0.4 V. The R₂ for the Cu-Sn foam in the CO₂ atmosphere is smaller than that in the N₂ one, which significantly indicates that Cu-Sn foam is more active for the CO₂RR. In contrast, the R₂ for the Cu foam in the CO₂ atmosphere becomes higher as compared to that in the N₂ atmosphere, indicating its lower activity for the CO₂RR. Therefore, the detailed EIS analysis confirms that the significant improvement in the selectivity for the CO₂RR can be expected on the Cu-Sn foam.

3.3. Product analysis of the CO₂RR on Cu and Cu-Sn foams

In order to confirm the activity and selectivity of the electrodes for the CO₂RR, CA measurements are carried out in a three-electrode two-compartment cell. During the tests, the Cu-Sn electrode achieves a lower current density compared to the Cu electrode at each fixed potential (Figure S4 of S.I.). This result is in consistence with CV and EIS analyses. The FE values of the major gas-phase products are determined when the concentrations reach stable values, while the FEs of the liquid products are calculated based on the concentrations in the electrolyte after 20 min of continuous reactions. As shown in Fig. 7a, the Cu electrode mainly produces H₂ at all tested potentials from -0.5 V to -1.0 V. The FE_{CO} reaches a maximum value of about 20% at the low and moderate overpotentials ($\eta = 390$ mV and 490 mV). With increasing the overpotential, the FE_{CO} value rapidly decreases, while the FE of the formic acid (FE_{HCOOH}) retains a constant value of about 18% from -0.6 V to -1.0 V. At higher overpotentials ($\eta \geq 890$ mV), other gas-phase products (not determined here) emerge, which agrees with the

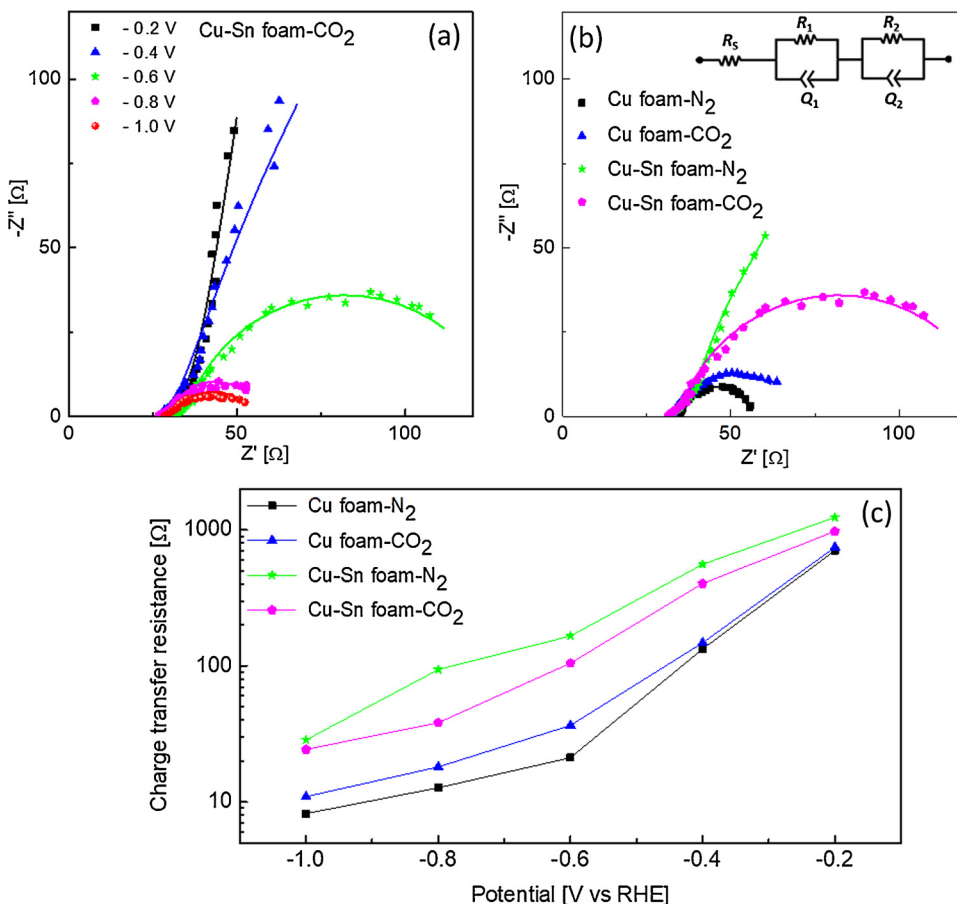


Fig. 6. EIS: (a) Nyquist plots related to Cu-Sn sample measured at different potentials in CO₂-saturated electrolyte (the points are experimental data, the lines are the curves calculated through a fitting procedure using the equivalent electrical circuit shown in the inset of (b)); (b) Impedance data acquired for Cu and Cu-Sn foams in CO₂- and N₂-bubbled electrolytes at -0.6 V vs RHE (the points are experimental data, the lines are the curves calculated through a fitting procedure using the equivalent electrical circuit shown in the inset); (c) Charge transfer resistances reported as a function of the potential.

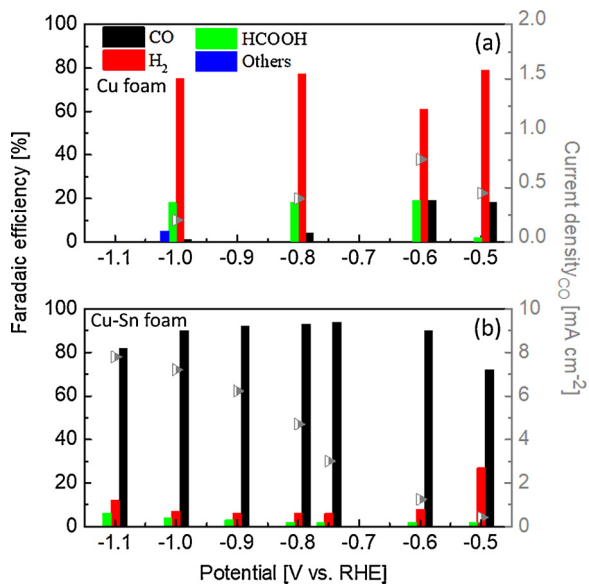


Fig. 7. Faradaic efficiencies of the major products and CO partial current densities at various potentials: (a) Cu electrode; (b) Cu-Sn electrode.

literature [33]. In addition, trace amount of acetic acid (CH₃COOH) and ethanol (C₂H₅OH) is also detected in the electrolyte after the test at each potential. The CO partial current densities on the Cu electrode are rather low despite the observed high total current densities, due to a low selectivity towards the CO production. In contrast, the Cu-Sn electrode exhibits an excellent selectivity towards the CO generation, as seen in Fig. 7b. CO is the main product from the CO₂RR and it is

characterized by a FE value of about 90% at -0.6 V (overpotential $\eta = 490$ mV). The FE_{CO} values are further enhanced up to 93–94 % under the overpotentials from 640 mV to 790 mV. At higher overpotentials ($\eta \geq 890$ mV), the FE_{CO} slowly drops down below 90%. The FEs for both the HER and the HCOOH formation are maintained at quite low values (FE_{H2} ≤ 8%; FE_{HCOOH} ≤ 5%) in a wide potential range from -0.6 V to -1.0 V. Moreover, no other liquid products, except HCOOH, are detected by NMR, and no other gas-phase products, except H₂ and CO, are expected since the total faradaic efficiency for the three observed products are almost 100%. Obviously, the introduction of the Sn species in the Cu foam has dramatically enhanced the selectivity towards the CO, meanwhile, it has efficiently prohibited the HER and the formation of other CO₂RR products. Besides the high FE_{CO}, the CO production also achieves a high partial current density of 1.2 mA cm⁻² at -0.6 V and rapidly increases up to 6.2 mA cm⁻² in the range of moderate overpotentials ($\eta = 490$ –790 mV). At high overpotentials ($\eta \geq 890$ mV), the increase rate of the CO current density becomes lower, meanwhile, the FE_{CO} value drops down, probably due to the limited mass transport of CO₂ in the system. However, such current densities are superior to the ones reported in other similar works [17,20].

Simultaneously obtained high CO selectivity and current densities demonstrate that the Cu-Sn foam is an efficient electrode for converting CO₂ to CO. We believe the remarkable selectivity can be attributed to the synergistic effect between Cu and Sn. According to Wang et al. [34], the Cu sites, assisted by the adjacent SnO_x sites, are responsible for the catalytic selectivity for CO. Electrons transfer from the oxide to the metal nanoparticles at the Cu/SnO_x interface, and the increased electron density on the Cu sites can weaken the binding of *CO and thus favors the CO₂ reduction to CO. Sun et al. [21] carried out density functional theory (DFT) calculation on the core-shell Cu@SnO₂ nanoparticles. It is stated that the high selectivity for CO can be attributed to the coexistence of the uniaxial compression and Cu atoms on the SnO₂

surface or subsurface. However, these explanations on the interaction of Cu and Sn are not suitable for the here studied Cu-Sn foam, since the active states of Cu and Sn elements in the foam are oxide-derived metallic species, as discussed in the next section. Takanabe et al. [17] investigated H adsorption on the single Sn atom decorated Cu (100) and (111) surfaces through the DFT calculation. They suggest that H does not bind to the Sn atom, and H adsorption on both modified Cu facets becomes much lower, with respect to that on the pure Cu structure. Therefore, more active sites participate in the CO₂RR instead of the HER. Our experimental results are in agreement with the above-mentioned theory, since the HER is dramatically suppressed on the Sn-modified Cu foam. In addition, CO₂RR on the Cu-Sn foam shows excellent selectivity for CO generation, and the formation of other products, such as HCOOH, CH₃COOH and C₂H₅OH, is prohibited. It is likely that the decrease of H adsorption on the surface also suppresses the hydrogenation of intermediates of the CO₂RR. The high current densities can be related to the hierarchical architecture of the Cu-Sn catalyst, which displays foam microstructure and dendritic nanostucture. A recent simulation work stated that the needle-like morphology can not only enhance the local reactant concentration but also improve the long-range CO₂ transport, effectively extending the electrode/solution interfaces [35]. It is also reported that nano-needle electrodes can produce local high electric fields that concentrate electrolyte cations, leading to a high local concentration of CO₂ which enables fast reduction reaction and achieves high reduction current [36].

3.4. Stability related studies on Cu-Sn foam

To study the stability of the Cu-Sn electrode, CO₂ electrolysis is carried out at one electrode at five applied potentials, with one or two hours at each potential. The total duration of the durability test is about 8 h. As shown in the Figure S5 of S.I., steady-state electrolysis current is observed at each applied potential. The FE_{CO} values and the CO production rates as a function of time are shown in Fig. 8. From Fig. 8a, quasi constant FE values are observed at moderate overpotentials (from -0.6 V to -0.9 V). At higher overpotentials, the oscillation of FE values can result from the rapid formation of gas bubbles which temporarily block part of the active interface, as already observed and reported in other electrochemical systems involving gaseous products [37,38]. The CO production rate increases with increasing the electrolysis potential (Fig. 8b), thereby following the steady-state electrolysis currents. At each potential, CO is produced at a quasi-constant rate due to the steady current and unaltered selectivity during the electrolysis. In addition, a long-term electrolysis of 10 h is conducted on the Cu-Sn electrode at -0.8 V in a dedicated system, as described and shown in the Figure S6 of S.I. The reductive current density is almost steady during the continuous operation, indicating the stable performance for the CO₂RR.

To further understand the active state and stability of the Cu-Sn foam, TEM, XRD and XPS analyses are performed on the Cu-Sn sample after the electrolysis. FESEM and STEM (in Figure S7a-c of S.I.) show that the Cu-Sn foam retains the dendritic morphology after the electrochemical tests. It is found that Cu₂O crystals of the shell are reduced to Cu, as supported by the electron diffraction (Figure S7d of S.I.) and XRD analysis (Figure S7e of S.I.). EDX analysis (not reported) confirms the coexistence of Cu and Sn. From XPS analysis (in Figure S8a of S.I.), it can be seen that the Cu2p signal has reduced noticeably the satellite intensity around 942 eV due to Cu(II), compared to the as-prepared sample. The Cu2p_{3/2} main peak has also reduced its full width at half maximum (FWHM), since most of the peak is attributed to the Cu(0) state. The Cu Auger peak (Figure S8b of S.I.) has moved towards higher kinetic energies at 918.8 eV, in accordance with the reported value of 918.6 eV for Cu(0) state [26]. In addition, on the tested sample, the modified Auger parameter is equal to 1851.0 eV comparable with the reported value of 1851.2 eV for metallic Cu [26]. As shown in Figure S8c, the Sn3d doublet has moved towards lower binding energies with a

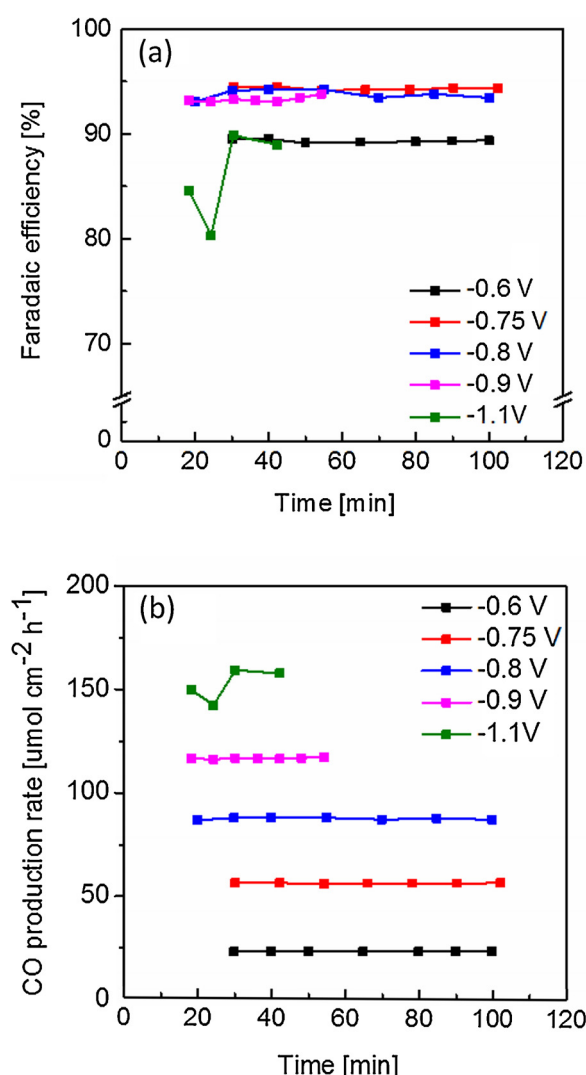


Fig. 8. CO₂ electrolysis carried out on the Cu-Sn electrode at various potentials: (a) Faradaic efficiencies; (b) CO production rate, as a function of time.

visible reduction of the FWHM, compared to the as-prepared sample, in accordance with the presence of the metallic state solely [17]. Therefore, the TEM and XPS analyses indicate that the oxides of Cu and Sn are unstable under the harsh reductive conditions of the CO₂ electrolysis, and the actually active state of the surface is composed of metallic species that derives from the oxides. The composition of the surface of the tested Cu-Sn foam is also examined by XPS analysis, and 2.9 at. % of Sn and a Cu/Sn atomic ratio of 8.8 are found. These values are comparable to the ones (2.2 at. % of Sn and a Cu/Sn atomic ratio of 8.9) detected on the surface of the as-prepared Cu-Sn foam. From these physical and chemical characterizations, it is believed that the surface of the foam is initially electrochemically reduced and then remains chemically and morphologically stable during the electrolysis.

From the positive observations of the stability tests, it is possible to state that the here developed Cu-Sn foam is a robust electrode with a high potential to be implemented in a real CO₂ electroreduction device.

4. Conclusions

A Cu-Sn catalyst with dendritic foam structure is simply prepared and carefully characterized employing several advanced surface analysis techniques. Due to deep understanding of the electrochemical analyses (CV and EIS), we successfully predict the high selectivity of Cu-Sn foam for the CO₂ conversion in aqueous electrolyte. By analyzing

the products, it is further confirmed that CO is the highly selected product from CO₂RR on the Cu-Sn catalyst. Excellent FE_{CO} values up to 93–94 % are obtained in a wide potential range (-0.75 V to -0.9 V vs RHE). High activity and stability of the hybrid electrode are also observed during the electrolysis. The present work highlights the importance of architecture and surface property of a catalyst for efficient CO₂ electroreduction. Three-dimensional dendrite foam structure facilitates mass transfer and benefits to the high reaction rate. The interaction of Cu and Sn results in outstanding selectivity for the CO formation. This can be an indication for developing efficient and sustainable electrocatalysts for large-scale electrolysis of CO₂.

Acknowledgements

This research did not receive any specific grant from funding agencies in the public, commercial, or not-for-profit sectors.

Appendix A. Supplementary data

Supplementary material related to this article can be found, in the online version, at doi:<https://doi.org/10.1016/j.apcatb.2018.05.056>.

References

- [1] J.W. Vickers, D. Alfonso, D.R. Kauffman, Energy Technol. 5 (2017) 1–22.
- [2] G. Centi, E.A. Quadrelli, S. Perathoner, Energy Environ. Sci. 6 (2013) 1711–1731.
- [3] E.V. Kondratenko, G. Mul, J. Baltrusaitis, G.O. Larrazabal, J. Perez-Ramirez, Energy Environ. Sci. 6 (2013) 3112–3135.
- [4] Z.-L. Wang, C. Li, Y. Yamauchi, Nano Today 11 (2016) 373–391.
- [5] R.J. Lim, M.S. Xie, M.A. Sk, J.M. Lee, A. Fisher, X. Wang, K.H. Lim, Catal.Today 233 (2014) 169–180.
- [6] K.P. Kuhl, T. Hatsukade, E.R. Cave, D.N. Abram, J. Kibsgaard, T.F. Jaramillo, J. Am. Chem. Soc. 136 (2014) 14107–14113.
- [7] D.D. Zhu, J.L. Liu, S.Z. Qiao, Adv. Mater. 28 (2016) 3423–3452.
- [8] G. Zhao, X. Huang, X.X. Wang, X.K. Wang, J. Mater. Chem. A 5 (2017) 21625–21649.
- [9] S. Lee, J. Lee, ChemSusChem 9 (2016) 333–344.
- [10] R. Kortlever, J. Shen, K.J.P. Schouten, F. Calle-Vallejo, M.T.M. Koper, J. Phys. Chem. Lett. 6 (2015) 4073–4082.
- [11] W. Zhu, Y.-J. Zhang, H. Zhang, H. Lv, Q. Li, R. Michalsky, A.A. Peterson, S. Sun, J. Am. Chem. Soc. 136 (2014) 16132–16135.
- [12] S. Hernández, M.A. Farkhondehhal, F. Sastre, M. Makkee, G. Saracco, N. Russo, Green. Chem. 19 (2017) 2326–2346.
- [13] J. Qiao, Y. Liu, F. Hong, J. Zhang, Chem. Soc. Rev. 43 (2014) 631–675.
- [14] K.P. Kuhl, E.R. Cave, D.N. Abram, T.F. Jaramillo, Energy Environ. Sci. 5 (2012) 7050–7059.
- [15] G.O. Larrazábal, A.J. Martín, S. Mitchell, R. Hauer, J. Pérez-Ramírez, ACS Catal. 6 (2016) 6265–6274.
- [16] A. Jedidi, S. Rasul, D. Masih, L. Cavallo, Takanabe K, J. Mater. Chem. A 3 (2015) 19085–19092.
- [17] S. Sarfraz, A.T. Garcia-Esparza, A. Jedidi, L. Cavallo, K. Takanabe, ACS Catal. 6 (2016) 2842–2851.
- [18] M. Tsuji, S. Hikino, R. Tanabe, M. Matsunaga, Y. Sanod, CrystEngComm. 12 (2010) 3900–3908.
- [19] G.O. Larrazábal, A.J. Martín, F. Krumeich, R. Hauer, J. Pérez-Ramírez, ChemSusChem 10 (2017) 1255–1265.
- [20] Y. Zhao, C. Wang, G.G. Wallace, J. Mater. Chem. A 4 (2016) 10710–10718.
- [21] Q. Li, J. Fu, W. Zhu, Z. Chen, B. Shen, L. Wu, Z. Xi, T. Wang, G. Lu, J. Zhu, S. Sun, J. Am. Chem. Soc. 139 (2017) 4290–4293.
- [22] H.-C. Shin, J. Dong, M. Liu, Adv. Mater. 15 (2003) 1610–1614.
- [23] A. Dutta, M. Rahaman, N.C. Luedi, M. Mohos, P. Broekmann, ACS Catal. 6 (2016) 3804–3814.
- [24] H. Xu, J.-X. Feng, Y.-X. Tong, G.-R. Li, ACS Catal. 7 (2017) 986–991.
- [25] C.K. Li, M.W. Kanan, J. Am. Chem. Soc. 134 (2012) 7231–7234.
- [26] M.C. Biesinger, L.W.M. Lau, A.R. Gerson, R.St.C. Smart, Appl. Surf. Sci. 257 (2010) 887–898.
- [27] A. Radi, D. Pradhan, Y. Sohn, K.T. Leung, ACS Nano 4 (2010) 1553–1560.
- [28] M.C. Biesinger, Surf. Interface Anal. 49 (2017) 1325–1334.
- [29] M.F. Baruch, J.E. Pander III, J.L. White, A.B. Bocarsly, ACS Catal. 5 (2015) 3148–3156.
- [30] D. Kim, S. Lee, J.D. Ocon, B. Jeong, J.K. Lee, J. Lee, Phys. Chem. Chem. Phys. 17 (2015) 824–830.
- [31] H. Ooka, M.C. Figueiredo, M.T.M. Koper, Langmuir 33 (2017) 9307–9313.
- [32] A. Sacco, Renew. Sustain. Energy Rev. 79 (2017) 814–829.
- [33] K. Chen, X. Zhang, T. Williams, L. Bourgeois, D.R. MacFarlane, Electrochim. Acta 239 (2017) 84–89.
- [34] S. Huo, Z. Weng, Z. Wu, Y. Zhong, Y. Wu, J. Fang, H. Wang, ACS Appl. Mater. Interfaces 9 (2017) 28519–28526.
- [35] T. Burdyny, P.J. Graham, Y. Pang, C.-T. Dinh, M. Liu, E.H. Sargent, D. Sinton, ACS Sustain. Chem. Eng. 5 (2017) 4031–4040.
- [36] M. Liu, Y. Pang, B. Zhang, P. De Luna, O. Voznyy, J. Xu, X. Zheng, C.T. Dinh, F. Fan, C. Cao, F.P. García de Arquer, T.S. Safaei, A. Mepham, A. Klinkova, E. Kumacheva, T. Fillette, D. Sinton, S.O. Kelley, E.H. Sargent, Nature 537 (2016) 382–386.
- [37] S. Hernández, G. Barbero, G. Saracco, A.L. Alexe-Ionescu, J. Phys. Chem. C 119 (2015) 9916–8825.
- [38] C. Torra, E. Lorente, S. Hernández, N. Russo, J. Salvadó, Fluids 2 (2017) 25–48.